5-26-2022

Numerical Solutions of a Gradient-Elastic Kirchhoff Plate Model on Convex and Concave Geometries Using Isogeometric Analysis

Yu Leng

Tianyi Hu

Sthavishtha R. Bhopalam

Hector Gomez

Journal of Mechanics, 2022, **38**, 238–249
https://doi.org/10.1093/jom/ufac017
Regular Article

Numerical solutions of a gradient-elastic Kirchhoff plate model on convex and concave geometries using isogeometric analysis

Yu Leng[1], Tianyi Hu[1], Sthavishtha R. Bhopalam[1] and Hector Gomez [1,*]

[1]School of Mechanical Engineering, Purdue University, West Lafayette, IN 47907, United States

*Corresponding author: hectorgomez@purdue.edu

ABSTRACT

In this work, we study numerical solutions of a gradient-elastic Kirchhoff plate model on convex and concave geometries. For a convex plate, we first show the well-posedness of the model. Then, we split the sixth-order partial differential equation (PDE) into a system of three second-order PDEs. The solution of the resulting system coincides with that of the original PDE. This is verified with convergence studies performed by solving the sixth-order PDE directly (*direct method*) using isogeometric analysis (IGA) and the system of second-order PDEs (*split method*) using both IGA and C^0 finite elements. Next, we study a concave pie-shaped plate, which has one re-entrant point. The well-posedness of the model on the concave domain is proved. Numerical solutions obtained using the split method differ significantly from that of the direct method. The split method may even lead to nonphysical solutions. We conclude that for gradient-elastic Kirchhoff plates with concave corners, it is necessary to use the direct method with IGA.

KEYWORDS: gradient-elastic Kirchhoff plate, isogeometric analysis, concave corners, sixth-order PDE

1. INTRODUCTION

Classical continuum mechanics has been successfully applied to macro-scale problems in civil [1], mechanical [2], material [3], structural engineering [4] and more [5,6]. Many of these problems exhibit multi-scale features and have broad engineering applications [7,8]. To study such problems, it is necessary to adopt a continuum theory, which includes multi-scale effects. However, the standard theory of continuum mechanics does not consider the internal length scale of the material at the micro- or nano-scale. Enrichment or modification of the classical theory becomes important to study problems across multiple scales. The theory of strain gradient elasticity [9,10] considers the effects of micro-structures using gradients of strains and requires the identification of more material parameters. Simplified models are developed to reduce the number of higher-order terms as well as material coefficients [11]. These models can capture the size effects of the material [12–14]. In this work, we are interested in numerical solutions of a simplified one-parameter gradient-elastic Kirchhoff plate model developed in [15].

The gradient-elastic Kirchhoff plate model is a sixth-order partial differential equation (PDE) in terms of the transverse deflection. If the sixth-order PDEs are solved directly (*direct method*), H^3-conforming finite element methods (FEMs) become necessary. Isogeometric analysis (IGA) [16], which offers basis functions with high-order inter-element continuity, is an ideal candidate for solving third- and higher-order PDEs [17–19], including the gradient-elastic Kirchhoff plate model [20–22]. There are other numerical methods [23–25] based on the direct method. Another approach that is widely used to solve third- and higher-order PDEs is the *split method* [26–32]. By rewriting any third- or higher-order PDE into a system of first- or second-order PDEs, the use of classical C^0 FEM becomes possible. Reformulating the biharmonic equation into two Poisson equations is an example of the split method. In this work, we will use both methods (direct and split) along with IGA and C^0 FEM to solve the gradient-elastic Kirchhoff model.

Previous works [21–25] on gradient-elastic Kirchhoff plate models are limited to convex geometries. Geometries with finitely many concave corners are important as they appear in many engineering applications. Can one expect numerical solutions obtained from the direct and split methods on convex and concave geometries to be the same? For the biharmonic equation, solutions obtained using the two methods differ in domains with concave corners [19,33–35]. We will borrow the ideas and tools from analysing the biharmonic equation to study how the direct and split methods perform on the gradient-elastic Kirchhoff plate model on both convex and concave geometries.

In this work, we study numerical solutions of the gradient-elastic Kirchhoff plate model with both convex and concave geometries using direct and split methods. We first show the well-posedness of the model when the plate is convex. Then, we split the sixth-order PDE into a system of three second-order

Received: 3 December 2021; **Revised:** 18 April 2022

PDEs, which enables the use of classical C^0 FEM. For concave pie-shaped geometries, the existence of a unique solution of the model is also provided. We solve the sixth-order PDE directly using IGA and the system of second-order PDEs using both IGA and C^0 FEM. Convergence studies of direct and split methods are performed, and the observed convergence rates are in good agreement with [21]. Next, numerical examples on a concave pie-shaped domain are presented. Numerical solutions obtained using the split method differ significantly from that of the direct method. The split method leads to nonphysical solutions for certain loads. Thus, for plates with concave corners, it is necessary to use the direct method with IGA.

This paper is organized as follows. In Section 2, the gradient-elastic Kirchhoff plate model, along with the direct and split formulations, is presented. Section 3 discusses discretization methods. Convergence studies on a convex domain and numerical examples on an pie-shaped domain are shown in Section 4. Finally, conclusions are made in Section 5.

2. GRADIENT-ELASTIC KIRCHHOFF PLATE MODEL

In this section, we first present the gradient-elastic Kirchhoff plate model. Then we discuss two methods to obtain a solution.

2.1 Model equation

We briefly present the gradient-elastic Kirchhoff plate model, and we refer readers to [36] for a detailed derivation. Let the plate occupy a three-dimensional domain $\Omega \times (-t/2, t/2)$, where the mid-surface of the plate is denoted as $\Omega \subset \mathbb{R}^2$, and $0 < t \ll \mathrm{diam}(\Omega)$ is the thickness of the plate. We assume Ω is open and bounded. In addition, t is assumed to be constant.

Let $w : \Omega \to \mathbb{R}$ be the transverse deflection of the mid-surface. A standard argument of dimension reduction techniques gives the gradient-elastic Kirchhoff plate model equation [21,36] as

$$D\Delta^2 w - g^2 D\Delta^3 w = f \text{ in } \Omega, \tag{1}$$

where $D = Et^3/[12(1-\nu^2)]$. Here, E and ν are Young's modulus and Poisson ratio of the material, g is a constant that represents the length scale of the micro-structure of the material and is also called the gradient parameter and f is the transverse body load scaled by the thickness of the plate. In order to have a well-posed boundary value problem, we need to provide Eq. (1) with boundary conditions.

Boundary conditions for strain-gradient elastic plates are nontrivial, and there are a number of options [11,37]. In this work, we are mainly interested in numerical solutions of the gradient-elastic Kirchhoff plate model on both convex and concave domains using the direct and split methods. For simplicity, we supply Eq. (1) with the following boundary conditions and formulate the model as

$$\Delta^2 w - g^2 \Delta^3 w = \hat{f} \text{ in } \Omega, \tag{2a}$$

$$w = \overline{w} \text{ on } \partial\Omega, \tag{2b}$$

$$-\Delta w + g^2 \Delta^2 w = \widehat{M}^g_{nn} \text{ on } \partial\Omega, \tag{2c}$$

$$g^2 \nabla\Delta w \cdot \boldsymbol{n} = \widehat{G}^g_{nn} \text{ on } \partial\Omega, \tag{2d}$$

where $\hat{f} = f/D, \overline{w}, \widehat{M}^g_{nn}, \widehat{G}^g_{nn}$ are given data, and $\boldsymbol{n}$ is the unit vector in outward normal direction to $\partial\Omega$.

Remark 1 1. *For a rectangular plate, when $g = 0$, the gradient-elastic model in Eq. (2) is equivalent to the classical simply supported Kirchhoff plate model* [36].
2. *The boundary value problem in Eq. (2) is well-posed and can be split into a system of equations that has a unique solution.*
3. *Boundary conditions of Eqs. (2c) and (2d) can be imposed naturally in the weak forms of the direct and split methods to be presented later.*

By differentiating convex and concave geometries, we discuss the next two methods, namely direct and split methods, to solve Eq. (2), and show the well-posedness of the problem on convex geometries and the existence of a solution on a special type of concave geometries.

2.2 Convex geometries

2.2.1 *Direct method on convex geometries*

We introduce more notations that are used throughout the paper. The standard L^2 inner product in Ω for scalar- or vector-valued quantities is denoted as $(\cdot,\cdot)$, and $\langle\cdot,\cdot\rangle$ is the duality pairing on the boundary, $\partial\Omega$. L^2 and $H^s(s>0)$ denote the classical Lebesgue and Sobolev spaces, respectively. Without loss of generality, we further assume $\overline{w} = \widehat{M}^g_{nn} = \widehat{G}^g_{nn} = 0$ for the rest of this section.

A weak solution of Eq. (2) is said to satisfy the following: find $w \in H^3(\Omega) \cap H^1_0(\Omega)$, such that

$$(\Delta w, \Delta v) + g^2(\nabla\Delta w, \nabla\Delta v) - (\hat{f}, v) = 0, \quad \forall v \in H^3(\Omega) \cap H^1_0(\Omega). \tag{3}$$

It is shown in [36] that Eq. (1) equipped with fully clamped boundary conditions is well-posed. We present next the well-posedness of the gradient-elastic Kirchhoff plate model with the boundary conditions given in Eq. (2).

Proposition 1. *Suppose Ω is convex. For every $\hat{f} \in L^2(\Omega)$, Eq. (2) has a unique solution $w \in H^3(\Omega) \cap H^1_0(\Omega)$, such that*

$$\|w\|_{H^3(\Omega)} \le C(\Omega, g)\|\hat{f}\|_{L^2(\Omega)}, \tag{4}$$

where $C(\cdot) > 0$ is a constant depending on $(\cdot)$.

Proof. As shown in [38, Chapter 8] for $w \in H^3(\Omega) \cap H^1_0(\Omega)$ the norm defined as $\|w\| := \|w\|_{H^2(\Omega)} + \|\Delta w\|_{H^1(\Omega)}$ is equivalent to $\|w\|_{H^3(\Omega)}$. Therefore,

$$\begin{aligned}\|w\|^2_{H^3(\Omega)} &\le C(\Omega)\left(\|w\|^2_{H^2(\Omega)} + \|\Delta w\|^2_{H^1(\Omega)}\right)\\ &\le C(\Omega)\left(\|\Delta w\|^2_{L^2(\Omega)} + \|\nabla\Delta w\|^2_{L^2(\Omega)}\right)\\ &\le C(\Omega,g)\left((\Delta w,\Delta w) + g^2(\nabla\Delta w,\nabla\Delta w)\right)\\ &= C(\Omega,g)(\hat{f},w)\\ &\le C(\Omega,g)\|\hat{f}\|_{L^2(\Omega)}\|w\|_{L^2(\Omega)}. \end{aligned} \tag{5}$$

Herein, from the first to the second line of Eq. (5), we have used the fact [38–40] that for $w \in H^2(\Omega)\cap H^1_0(\Omega)$

$$\|w\|_{H^2(\Omega)} \le C(\Omega)\|\Delta w\|_{L^2(\Omega)}. \tag{6}$$

□

2.2.2 *Split method on convex geometries*

The direct method discussed in the previous section requires $w \in H^3$ which prohibits the use of classical C^0 FEM. We introduce a split method [26–32,35] commonly used for third- and higher-order PDEs in this section.

By introducing, $u_1 = -\Delta w$ and $u_2 = u_1 - g^2\Delta u_1$, Eq. (2) can be rewritten into the a system of three second-order boundary-value problems

$$\begin{cases} -\Delta u_2 = \hat{f} \text{ in } \Omega, \\ u_2 = 0 \text{ on } \partial\Omega, \end{cases} \quad \begin{cases} u_1 - g^2\Delta u_1 = u_2 \text{ in } \Omega, \\ \nabla u_1 \cdot \boldsymbol{n} = 0 \text{ on } \partial\Omega, \end{cases}$$

$$\begin{cases} -\Delta w = u_1 \text{ in } \Omega, \\ w = 0 \text{ on } \partial\Omega. \end{cases} \tag{7}$$

Before discussing the solution of Eq. (7), we define the functional space

$$\mathcal{U} = H^1_0(\Omega)\times H^1(\Omega)\times H^1_0(\Omega). \tag{8}$$

A weak form of Eq. (7) is: find $(u_2,u_1,w)\in\mathcal{U}$, such that

$$\begin{aligned}(\nabla u_2,\nabla v_2) - (\hat{f},v_2) + (u_1,v_1) + g^2(\nabla u_1,\nabla v_1)\\ - (u_2,v_1) + (\nabla w,\nabla v_0) - (u_1,v_0)\\ = 0,\ \forall (v_2,v_1,v_0)\in\mathcal{U}.\end{aligned} \tag{9}$$

Eq. (9) can also be written as: find $(u_2,u_1,w)\in\mathcal{U}$, such that

$$(\nabla u_2,\nabla v_2) - (\hat{f},v_2) = 0, \quad \forall v_2 \in H^1_0(\Omega), \tag{10a}$$

$$(u_1,v_1) + g^2(\nabla u_1,\nabla v_1) - (u_2,v_1) = 0, \quad \forall v_1 \in H^1(\Omega), \tag{10b}$$

$$(\nabla w,\nabla v_0) - (u_1,v_0) = 0, \quad \forall v_0 \in H^1_0(\Omega). \tag{10c}$$

From classical results for elliptic boundary value problems [41] one can show that Eq. (7) is well-posed by successively solving the system of equations in (10).

Corollary 1. *Suppose Ω is convex. If $\hat{f}\in L^2(\Omega)$ then Eq. (7) has a unique solution $w\in H^2(\Omega)\cap H^1_0(\Omega)$ with $\Delta w \in H^2(\Omega)$ and $-\Delta w + g^2\Delta^2 w \in H^2(\Omega)\cap H^1_0(\Omega)$.*

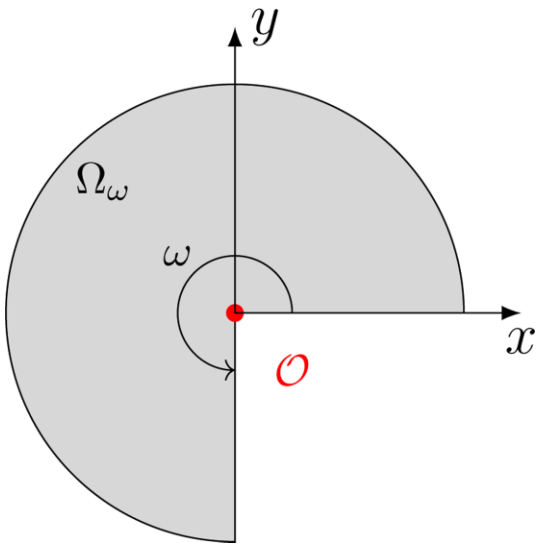

Figure 1 Pie-shaped domain Ω_ω with one re-entrant point $\mathcal{O}=(0,0)$ for $\pi < \omega < 2\pi$.

Remark 2. *For convex Ω and $\hat{f}\in L^2(\Omega)$, the solutions of Eqs. (2) and (7) coincide. Using numerical examples, we will verify that numerical solutions of Eqs. (2) and (7) converge to the same solution.*

Remark 3. *As shown in Eq. (5), the stability constant depends on g. The coercivity constant in Eq. (10b) also depends on g. We will explore how the solution behaves with different g using numerical examples.*

2.3 Concave geometries

For less regular domains such as domains with finitely many concave corners, one can not expect solutions of Eqs. (2) and (7) to be the same. Without loss of generality, we consider a pie-shaped domain with only one re-entrant point as shown in Fig. 1. In this section, we assume $\omega\in(\pi,2\pi)$, and replace Ω with Ω_ω. It is convenient to express Ω_ω in polar coordinates, namely

$$\Omega_\omega = \{(r,\theta) : r\in(0,1) \text{ and } \theta\in(0,\omega)\} \tag{11}$$

where the transformation from polar coordinates $\boldsymbol{x}=(r,\theta)\in\Omega_\omega$ to Cartesian coordinates $\boldsymbol{x}=(x,y)\in\Omega_\omega$ is defined as

$$\begin{cases} x = r\cos\theta, \\ y = r\sin\theta. \end{cases} \tag{12}$$

Because we do not expect solutions of direct method Eq. (3) and split method Eq. (9) to be the same on Ω_ω, we differentiate them as w^d and w^s, respectively. We next present the uniqueness of w^s followed by the existence of w^d.

2.3.1 *Split method*

The existence and uniqueness of a solution w^s for the split method on concave geometries is the same as Section 2.2.2. We rewrite Eqs. (10a) and (10b) using operators $\mathcal{G}: L^2(\Omega_\omega)\to H^1_0(\Omega_\omega)$ and $\mathcal{G}_g: L^2(\Omega_\omega)\to H^1(\Omega_\omega)$, respectively,

$$u_2 = \mathcal{G}\hat{f}\in H^1_0(\Omega_\omega), \text{ and } u_1 = \mathcal{G}_g u_2 = \mathcal{G}_g\mathcal{G}\hat{f}\in H^1(\Omega_\omega), \tag{13}$$

Similarly, Eq. (10c) can be written as

$$w^s = \mathcal{G}u_1 = \mathcal{G}\mathcal{G}_g\mathcal{G}\hat{f} \in H_0^1(\Omega_\omega). \tag{14}$$

2.3.2 Direct method

On concave domains with re-entrant points, we cannot use the technique adopted in Proposition 1. By following [33,34,42] we instead show in this section that for a given $\hat{f}$ there exists a unique solution in $H^3(\Omega_\omega) \cap H_0^1(\Omega_\omega)$ that satisfies Eq. (3). We first introduce a series of functions

$$u_{\omega j} = \left(r^{-j\pi/\omega} - r^{j\pi/\omega}\right) \sin\left(j\pi\theta/\omega\right), \quad j \in \mathbb{Z}^+. \tag{15}$$

We note that $u_{\omega,j} \in L^2(\Omega_\omega)$ but $u_{\omega,j} \notin H^1(\Omega_\omega)$. It is easy to check that $u_{w,j}$ satisfies the following,

$$\begin{cases} -\Delta u_{\omega,j} = 0, \text{ in } \Omega_\omega, \\ u_{\omega,j} = 0, \text{ on } \partial\Omega_\omega \backslash \{\mathcal{O}\}. \end{cases} \tag{16}$$

Next, we show the well-posedness of the gradient-elastic Kirchhoff plate model Eq. (2) on the pie-shaped domain Ω_ω.

Theorem 1. *Provided $\hat{f} \in L^2(\Omega_\omega)$, there exists a unique solution $w^d \in H^3(\Omega_\omega) \cap H_0^1(\Omega_\omega)$ satisfying Eq. (3).*

Proof. Adding Eq. (15) to u_2 and following a similar procedure as in Section 2.3.1, we obtain

$$\begin{aligned} u_2^d &= \mathcal{G}\hat{f} + \sum_{j\in\mathbb{Z}^+} d_j u_{\omega,j} \\ &= u_2 + \sum_{j\in\mathbb{Z}^+} d_j u_{\omega,j} \in L^2(\Omega_\omega), \end{aligned} \tag{17}$$

$$\begin{aligned} u_1^d &= \mathcal{G}_g\mathcal{G}\hat{f} + \sum_{j\in\mathbb{Z}^+} d_j \mathcal{G}_g u_{\omega,j} \\ &= u_1 + \sum_{j\in\mathbb{Z}^+} d_j \mathcal{G}_g u_{\omega,j} \in H^1(\Omega_\omega), \end{aligned} \tag{18}$$

$$\begin{aligned} w^d &= \mathcal{G}\mathcal{G}_g\mathcal{G}\hat{f} + \sum_{j\in\mathbb{Z}^+} d_j \mathcal{G}\mathcal{G}_g u_{\omega,j} \\ &= w^s + \sum_{j\in\mathbb{Z}^+} d_j \mathcal{G}\mathcal{G}_g u_{\omega,j} \in H_0^1(\Omega_\omega), \end{aligned} \tag{19}$$

for some coefficients $d_j \in \mathbb{R}$. For the split method, $d_j = 0$ for $j \in \mathbb{Z}^+$ because it is required that $u_2^d = -\Delta w^d + g^2\Delta^2 w^d \in H^1(\Omega_\omega)$. However, we show next that there are non-zero d_j such that $w^d \in H^3(\Omega_\omega)$.

Because $u_1^d \in H^1(\Omega_\omega)$ [42, Lemma 6.6.1], the weak solution of the Laplacian problem with Dirichlet boundary conditions on Ω_ω, namely $\mathcal{G}u_1^d$, possesses the asymptotic expansion [43, Theorem 3.4], [42, Theorem 6.6.1]

$$\begin{aligned} w^d(\boldsymbol{x}) &= \chi(r) \sum_{i=1}^{3} c_i r^{i\pi/\omega} \sin\left(i\pi\theta/\omega\right) + \widetilde{w}(\boldsymbol{x}), \\ &\text{for } \widetilde{w} \in H^3(\Omega_\omega) \cap H_0^1(\Omega_\omega), \end{aligned} \tag{20}$$

where

$$\begin{aligned} \chi \in C^\infty(\mathbb{R}) \text{ satisfies } \chi(r) \\ = \begin{cases} 1, & \text{for } r \le 0.5, \\ 0 & \text{for } r \ge 1, \end{cases} \text{ and } 0 \le \chi < 1, \end{aligned} \tag{21}$$

and

$$c_i = \left(\left(\mathcal{G}_g\mathcal{G}\hat{f} + \sum_{j\in\mathbb{Z}^+} d_j \mathcal{G}_g u_{\omega,j} \right), u_{\omega,i} \right), \text{ for } j = 1, 2, 3. \tag{22}$$

If $w^d \in H^3(\Omega_\omega) \cap H_0^1(\Omega_\omega)$, then we obtain

$$0 = c_i = \left(\left(\mathcal{G}_g\hat{f} + \sum_{j\in\mathbb{Z}^+} d_j \mathcal{G}_g u_{\omega,j} \right), u_{\omega,i} \right). \tag{23}$$

Using Parseval's identity and Fourier analysis, we have $(\mathcal{G}_g u_{w,j}, u_{w,j}) \neq 0$, for $j = 1, 2, 3$. Then Eq. (23) leads to

$$d_j = \begin{cases} -\dfrac{(\mathcal{G}_g\mathcal{G}\hat{f}, u_{\omega,j})}{(\mathcal{G}_g u_{\omega,j}, u_{\omega,j})}, & \text{for } j = 1, 2, 3, \\ 0, & \text{for } j \ge 4. \end{cases} \tag{24}$$

As a consequence, for a given $\hat{f} \in L^2(\Omega_\omega)$, w^d with d_j defined in Eq. (24) is in $H^3(\Omega_\omega) \cap H_0^1(\Omega_\omega)$, and satisfies Eq. (3). This completes the proof.

□

It is easy to see from Eq. (19) that w^d is different from the solution of the split method w^s. The H^1 solution w^s fails to capture additional terms as demonstrated in Eq. (19).

Remark 4. *The elliptic operator, $-\Delta w + cw$, $c \ge 0$, has maximum principle [39,42,43]. Therefore if $0 \le \hat{f} \in L^2(\Omega_\omega)$, then Eq. (14) also satisfies $w = \mathcal{G}\mathcal{G}_g\mathcal{G}\hat{f} \ge 0$. However, Eq. (19) does not have such a result because $d_j\mathcal{G}\mathcal{G}_g u_{\omega,j}$ can change signs on Ω_ω. We will show this discrepancy using numerical examples.*

3. DISCRETIZATION

We use the Galerkin method along with the two methods discussed in Sections 2.2.1 and 2.2.2 to solve the gradient-elastic Kirchhoff plate model. In this section, we describe the numerical methods used to discretize the weak forms obtained using the direct and split methods.

3.1 Spline basis

We briefly discuss the spline basis used in IGA, and refer to [16] for more details. Setting the weights of all control points to 1 we can reduce NURBS to B-splines. We will use tensor product basis functions. In this paper, we use bases with C^{p-1} continuous derivatives for B-splines of order $p \ge 1$.

3.2 IGA for direct method

As discussed in Section 2.2.1, it is necessary to use H^3-conforming functional spaces for the direct method. The weak

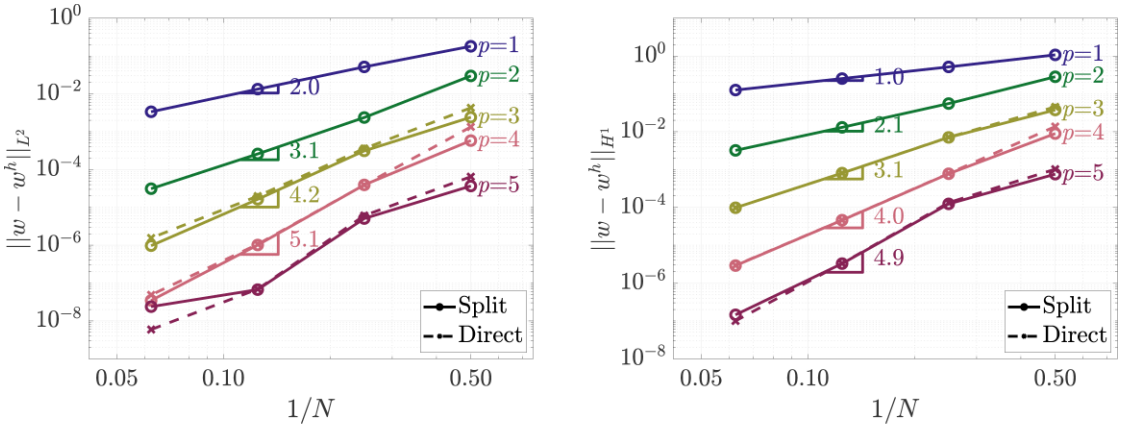

(a) $L^2(\Omega)$ (b) $H^1(\Omega)$

Figure 2 Convergence results of w in L^2 and H^1 norms using the split method (Section 3.3) with $g = 0.01$ for $p = 1, 2, \ldots, 5$. For comparison, convergence results of w using the direct method (Section 3.2) with $g = 0.01$ for $p = 3, 4, 5$, are also included.

form of Eq. (2) is given as: find $w^h \in H^3(\Omega)$, and $w^h = \overline{w}$ on $\partial\Omega$, such that

$$\left(\Delta w^h, \Delta v^h\right) + g^2\left(\nabla\Delta w^h, \nabla\Delta v^h\right) - \left(\hat{f}, v^h\right) - \left\langle \widehat{G}^g_{nn}, \Delta v^h\right\rangle + \left\langle \widehat{M}^g_{nn}, \nabla v^h \cdot \boldsymbol{n}\right\rangle = 0, \quad \forall v^h \in H^3(\Omega) \cap H^1_0(\Omega). \tag{25}$$

Note that for the rest of the paper, we relax the assumption of the boundary data, namely $\widehat{M}^g_{nn}$ and $\widehat{G}^g_{nn}$ do not have to be zero. As discussed in Remark 1, Eqs. (2c) and (2d) are imposed naturally in Eq. (25).

IGA uses spline basis functions (of order $p \geq 1$), which facilitates the construction of H^p-conforming approximation spaces, and has been used to discretize the gradient-elastic Kirchhoff plate model in [21]. We will use IGA ($p \geq 3$) to discretize Eq. (25).

3.3 IGA and C^0 finite elements for the split method

The split method proposed in Section 2.2.2 only requires the functional spaces to be H^1-conforming. The weak form of Eq. (7) is given by: find $(u^h_2 u^h_1, w^h) \in H^1(\Omega) \times H^1(\Omega) \times H^1(\Omega)$, $u^h_2 = \widehat{M}^g_{nn}$ and $w^h = \overline{w}$ on $\partial\Omega$, such that

$$\left(\nabla u^h_2, \nabla v^h_2\right) - \left(\hat{f}, v^h_2\right) + \left(u^h_1, v^h_1\right) + g^2\left(\nabla u^h_1, \nabla v^h_1\right) + \left\langle \widehat{G}^g_{nn}, v^h_1\right\rangle - \left(u^h_2, v^h_1\right) + \left(\nabla w^h, \nabla v^h_0\right) - \left(u^h_1, v^h_0\right) = 0, \quad \forall (v^h_2, v^h_1, v^h_0) \in \mathcal{U}. \tag{26}$$

The above equation confirms that Eqs. (2c) and (2d) can be imposed naturally in the weak form. For the split method it is sufficient to use classical C^0 finite elements, which are H^1-conforming. For the ease of implementation, we use IGA of order $p \geq 1$ to solve Eq. (26). We remark that IGA and C^0 finite elements coincide when $p = 1$.

4. NUMERICAL EXAMPLES

In this section, we present numerical examples using the direct and split methods discussed in the previous section to solve the gradient-elastic Kirchhoff plate model. We first perform convergence studies on a convex domain. Then, we study the pie-shaped plate.

4.1 Convergence study on convex domain

In this section, we choose $\Omega = (0, 1)^2$, and use a manufactured solution $w = \sin(\pi x)\sin(\pi y)$, which leads to the forcing function

$$\hat{f}(x, y) = 4\pi^4 \sin(\pi x)\sin(\pi y) + 8g^2\pi^6 \sin(\pi x)\sin(\pi y). \tag{27}$$

Thus, the boundary data become

$$\overline{w} = 0, \quad \widehat{M}^g_{nn} = 0, \quad \text{and} \quad \widehat{G}^g_{nn} = -2g^2\pi^3[\cos(\pi x)\sin(\pi y), \cos(\pi y)\sin(\pi x)] \cdot \boldsymbol{n}, \tag{28}$$

which are used in Eqs. (25) and (26). In this case, Ω is convex and $\hat{f} \in L^2(\Omega)$, thus as in Remark 2, we expect the solutions using direct (Section 3.2) and split (Section 3.3) methods coincide.

Convergence studies are performed using four uniform meshes. The number of elements in each direction is denoted as $N = 2, 4, 8$ and 16. On each mesh, we fix $g = 0.01$ and solve Eq. (26) equipped with Eqs. (27) and (28) for $p = 1, 2, \ldots, 5$. Numerical solutions are compared against the manufactured solution. Convergence results of w, u_1 and u_2 in L^2 and H^1 norms are reported in Figs. 2–4. In addition, Eq. (25) together with Eqs. (27) and (28) is solved for $p = 3, 4, 5$. Convergence results of w in L^2 and H^1 norms using the direct method are included in Fig. 2 for comparison with the split method. Convergence results of w in H^2 and H^3 norms using the direct method can be found in Appendix A.

As shown in Fig. 2a and b, convergence rates of w in L^2 and H^1 norms are optimal, namely for pth ($p \leq 4$) order B-splines, the convergence rates in L^2 and H^1 norms are of order $p + 1$ and p, respectively. Figures 3 and 4 indicate that optimal convergence rates of the additional variables u_1 and u_2 in L^2, and H^1 norms are also achieved for $p \leq 4$. When

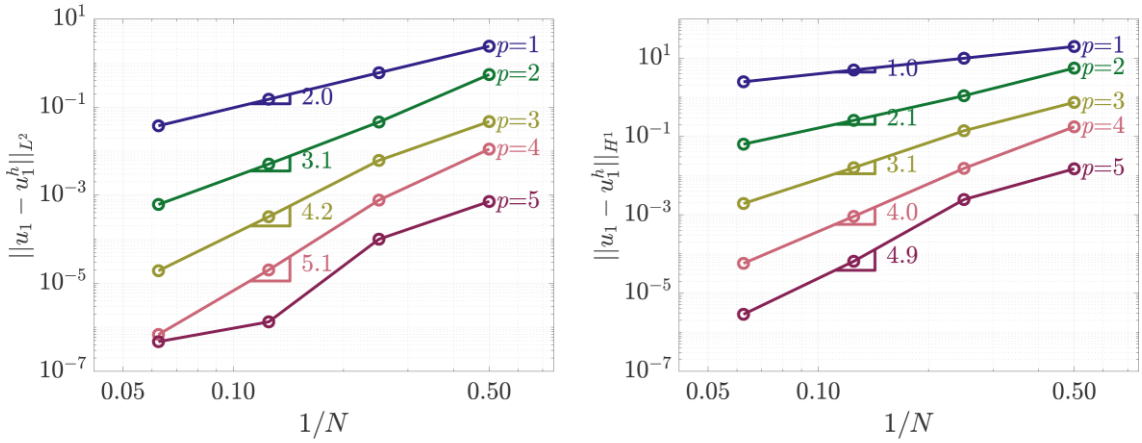

(a) $L^2(\Omega)$ (b) $H^1(\Omega)$

Figure 3 Convergence results of $u_1 = -\Delta w$ in L^2 and H^1 norms using the split method (Section 3.3) with $g = 0.01$ for $p = 1, 2, \ldots, 5$.

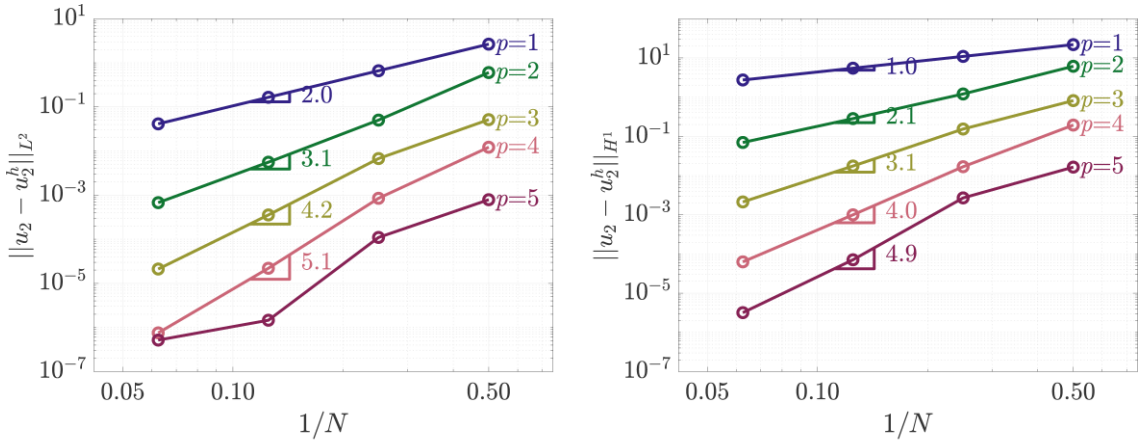

(a) $L^2(\Omega)$ (b) $H^1(\Omega)$

Figure 4 Convergence results of $u_2 = -\Delta w + g^2\Delta^2 w$ in L^2 and H^1 norms using the split method (Section 3.3) with $g = 0.01$ for $p = 1, 2, \ldots, 5$.

$p = 5$, convergence rates of w, u_1 and u_2 deteriorate in L^2 norm, see Figs. 2a, 3a and 4a, but they are optimal in H^1 norm, see Figs. 2b, 3b and 4b. As presented in Fig. 2a, convergence rates in L^2 norm using the direct method suffer from some deterioration, which has been observed in [21]. Convergence rates in H^1 H^2 and H^3 are optimal as shown in Appendix A. Therefore, we have verified that on convex domains, numerical solutions for the gradient-elastic Kirchhoff plate model using the direct and split methods converge to the same solution.

Next, we study the convergence behaviour using the split method with linear splines ($p = 1$) for fixed $g = 0.01, 0.05, 0.14$ and 0.20. As discussed in Remark 3, the stability constants of the direct and split methods depend on g. Thus, convergence rates with g-dependence are expected for both methods. It is observed in [21] that convergence rates of w in L^2 and H^1 norms using the direct method change slightly with g. On the contrary Fig. 5a and b shows that the convergence behaviour of w in L^2 and H^1 norms using the split method is independent of the gradient parameter g. This independence upon g is also true for u_1 and u_2, and more convergence results for different g are presented in Appendix B.

4.2 Concave pie-shaped domain

In this section, we consider the pie-shaped plate with $\omega = 10\pi/9$ and $3\pi/2$ as shown in Fig. 1. We use polar parametrization to represent the pie-shaped geometry [44]. For $\omega = 10\pi/9$ the control points used to generate the geometry with cubic splines are shown in Fig. 6a. The mesh, consisting of 256×802 elements, is demonstrated in Fig. 6b. The control points and mesh (256×905 elements) for $\omega = 3\pi/2$ are similar to Fig. 6, and thus are omitted for conciseness. We remark that the corresponding basis functions are H^3-conforming on $\Omega_\omega \backslash \mathcal{O}$. The inverse of the geometric mapping is singular at $\mathcal{O}$ due to repeated control points [45] such as e_{1-20}, which are shown in Fig. 6a.

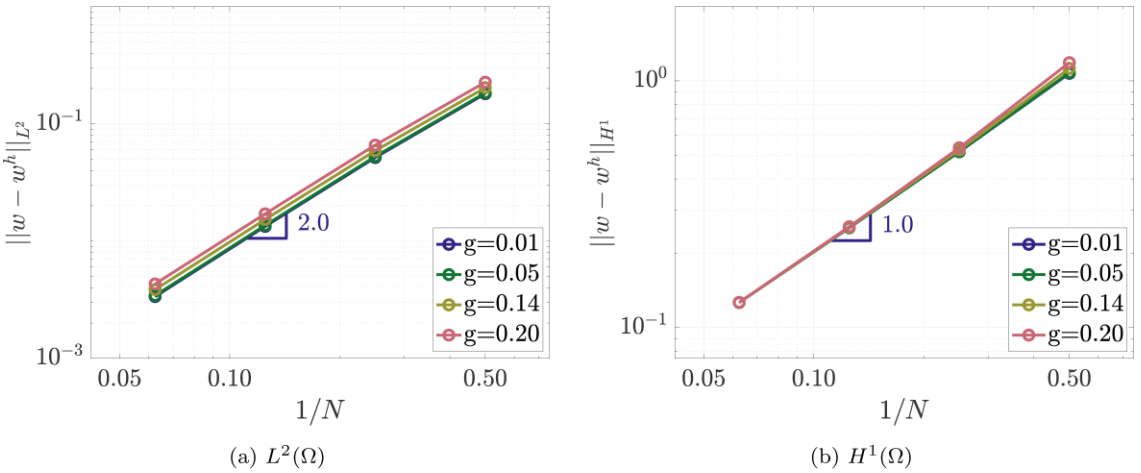

(a) $L^2(\Omega)$ (b) $H^1(\Omega)$

Figure 5 Convergence results of $u_1 = -\Delta w$ in L^2 and H^1 norms using the split method (Section 3.3) with $p = 1$ and $g = 0.01, 0.05, 0.14, 0.2$.

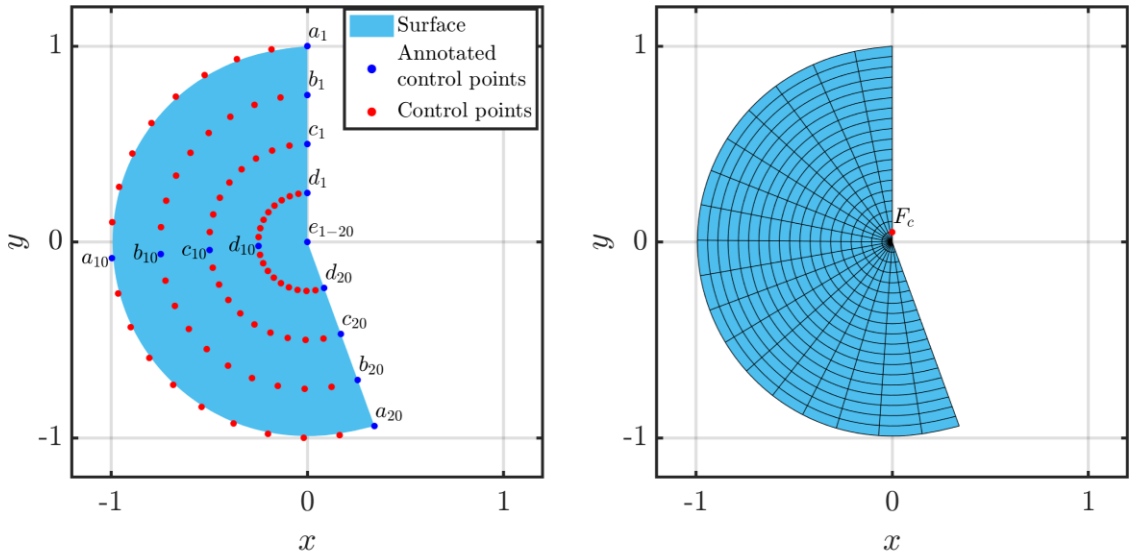

(a) Control points (b) Mesh

Figure 6 (a) A fraction of control points used to generate the pie-shaped geometry for $\omega = 10\pi/9$. Points $e_1, \ldots, e_{20}$ overlap with each other. In the simulation, 256 control points in the tangential direction and 5 control points in the radial direction are used to generate the geometry. (b) Mesh demonstration for $\omega = 10\pi/9$. In the simulation, the mesh has 256×802 elements.

Nevertheless, the use of Gaussian quadrature points avoid the evaluation of the basis function at the singular point $\mathcal{O}$. It is shown in [46] that polar parametrization on a sphere yields optimal convergence rates in H^3 norm for the solution of a sixth-order PDE. Thus we still use the resulting basis functions for the direct method.

We take $g = 0.01$ and $\overline{w} = \widehat{M}^g_{nn} = \widehat{G}^g_{nn} = 0$ for all numerical experiments in this section. A nonuniform body load acting on the pie-shaped plate is considered

$$\hat{f}(\boldsymbol{x}) = 10(-\tanh((d(\boldsymbol{x}) - 0.05)/0.01) + 1), \quad \boldsymbol{x} \in \Omega, \tag{29}$$

where $d(\boldsymbol{x}) = \sqrt{x^2 + (y - 0.05)^2}$, and $\boldsymbol{x} = (x, y)$. The nonuniform load, $\hat{f}$ in Eq. (29), which is centered at F_c in Fig. 6b, is non-negative and decays quickly to zero. We remark that the support of $\hat{f}$ is fully resolved by the mesh in Fig. 6b. First of all, we solve Eq. (25) on Ω_ω directly and denote the solution as $w^{d,h}$. Then, Eq. (26) is solved on the pie-shaped geometry so as to obtain w^s. Finally, following the procedure presented in Section 2.3.2 and utilizing w^s, we obtain the H^3 solution w^d in Eq. (19). The resulting transverse deflection is shown in Figs. 7a and 8a for $w^{d,h}$, in Figs. 7b and 8b for w^d and in Figs. 7c and 8c for w^s.

Note that the values of w^d that we will report are not exact as we can only evaluate Eq. (19) computationally. The computational process involves the approximation of w^s, the computation of the coefficients d_j in Eq. (24) and the computation of $\mathcal{G}\mathcal{G}_g u_{\omega,j}$. This entails the numerical approximation of the diffusion and reaction-diffusion problems with singular source terms. Thus, we do not expect a perfect agreement between w^d and

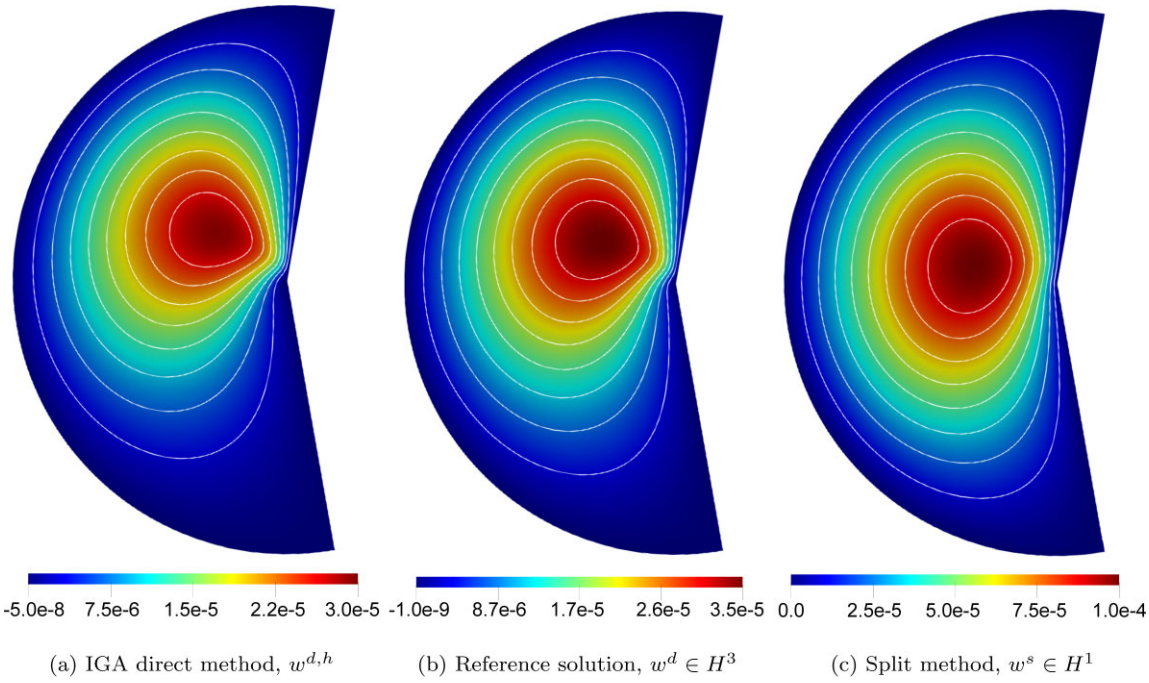

(a) IGA direct method, $w^{d,h}$ (b) Reference solution, $w^d \in H^3$ (c) Split method, $w^s \in H^1$

Figure 7 Numerical approximation to w obtained using the direct method in Section 3.2, reference solution in Section 2.3.2 and split method in Section 3.3 with $\omega = 10\pi/9$, and $g = 0.01$. Note that the deflection changes sign for the direct method and reference solution, but it is strictly positive for the split method.

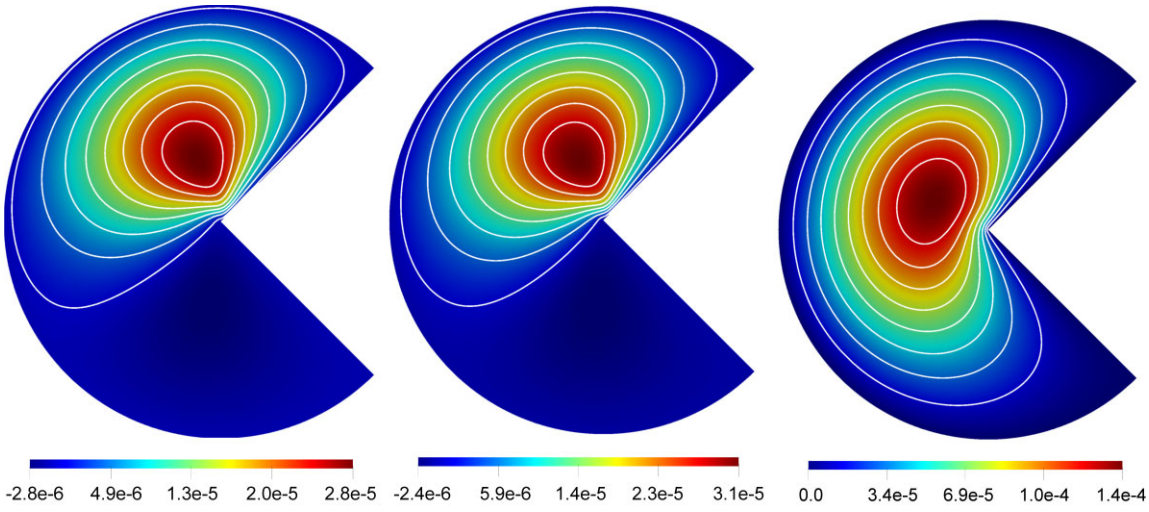

(a) IGA direct method, $w^{d,h}$ (b) Reference solution, $w^d \in H^3$ (c) Split method, $w^s \in H^1$

Figure 8 Numerical approximation to w obtained using the direct method in Section 3.2, reference solution in Section 2.3.2 and split method in Section 3.3 with $\omega = 3\pi/2$, and $g = 0.01$. Note that the deflection changes sign for the direct method and reference solution, but it is strictly positive for the split method.

$w^{d,h}$; but we do expect w^d and $w^{d,h}$ to be in good agreement and w^s to be fundamentally different. This is indeed what the results will show. Comparing Fig. 7a against Fig. 7b and Fig. 8a against Fig. 8b, we observe that the contour lines of $w^{d,h}$ and w^d are similar everywhere on Ω_ω especially near the singular point $\boldsymbol{x} = \mathbf{0}$. The good agreement of $w^{d,h}$ and w^d in contour lines justifies the use of the repeated control points at $\mathcal{O}$. However, the maximum values of transverse displacements, $w^{d,h}$ and w^d, are slightly different and show an error of $\sim$16% in Fig. 7, and of $\sim$10% in Fig. 8.

While w^d and $w^{d,h}$ are in good agreement, it is easy to see from Figs. 7 and 8 that the H^1 solution w^s differs significantly from $w^{d,h}$ and w^d. In particular, the contour lines near the concave corner $\boldsymbol{x} = \mathbf{0}$ of w^s are smoother than those of $w^{d,h}$ and w^d. In Fig. 7,

the maximum value of the displacement using the split method shows an error of $\sim 186\%$ with respect to w^d and an error of $\sim 233\%$ with respect to $w^{d,h}$. The difference between w^s and w^d or $w^{d,h}$ is even more dramatic in Fig. 8. The maximum transverse displacement from the split method shows an error of $\sim 340\%$ with respect to w^d and an error of $\sim 393\%$ with respect to $w^{d,h}$. This can be explained by that compared to w^d, the H^1 solution w^s excludes additional terms induced by the series of functions $u_{\omega,j}$ in Eq. (15), which are singular near the re-entrant point. Therefore, this shows that the H^1 solution of the split method cannot capture important features of the reference solution near the geometric singular point.

In addition, as shown in Fig. 7a and b, both the IGA direct solution $w^{d,h}$ and the reference solution w^d give a sign-changing transverse deflection near the concave corner. Meanwhile, Fig. 7c indicates that w^s is strictly positive everywhere in Ω_ω. The sign-changing effect is more evident in Fig. 8 when $w = 3\pi/2$. This can be explained using the maximum principle [39]. As stated in Remark 4, the elliptic operator, $-\Delta w + cw$, $c \geq 0$, has a maximum principle. Therefore, a positive load $\hat{f}$, such as in Eq. (29), leads to a positive u_2 in Eq. (13). As a result, u_1 in Eq. (13) is positive. Then, w^s obtained using Eq. (14) becomes positive. However, the sign of $w^d \in H^3$ in Eq. (19) depends on both $\hat{f}$ and the geometric singularity at the concave corners [34], namely the angle ω.

These results show the superiority of the direct method with IGA over the split method. The reason is 2-fold. First, the contour lines of the solution obtained using the direct method are similar to those of the reference solution, while the solution from the split method is very different from the reference solution. Second, for a positive body load, the reference solution and the solution from the direct method might change signs near the concave corner, while the split method results in a positive solution.

5. CONCLUSION

In this work, we have studied numerical solutions of a gradient-elastic Kirchhoff plate model. First, we assumed that the plate geometry is convex. We showed the well-posedness of the model in H^3. Then, we split the sixth-order PDE into a system of three second-order PDEs, and the resulting solution is only in H^1. The well-posedness of the system of equations is trivial, and the solutions obtained using the direct and split methods coincide. Next, we consider a pie-shaped domain with one re-entrant point. For any given data in L^2, the uniqueness of an H^3 solution of the model is proved by utilizing the H^1 solution, which is obtained by the system of second-order PDEs. The difference between the H^3 solution and the H^1 solution is presented.

The fact that the H^3 and H^1 solutions coincide on convex geometry is verified numerically by conducting convergence studies using a manufactured solution. Optimal convergence rates are obtained using the direct method along with IGA and the split method with IGA and C^0 FEM. In addition, for the range of the gradient parameters studied in this work, we observe an independence between the performance of the split method and the gradient parameter. However, it is found in [21] that convergence rates in L^2 and H^1 norms using the direct method depend moderately on the gradient parameter.

Next, numerical examples on a concave pie-shaped domain, which is subjected to a nonuniform body load, were studied. The transverse deflection obtained using the direct method agrees well with the reference solution. The H^1 solution, which is obtained using the split method, differs significantly from the reference solution in H^3. The deflection contour lines near the concave corner are also dissimilar. More importantly, for a positive nonuniform body load, the reference solution and the solution from the direct method both change signs near the concave corner, while the H^1 solution from the split method preserves the positivity. For plates with geometric singularities, it is hence necessary to use the direct method with IGA.

This work opens up a number of possibilities for future work. We have only considered a boundary condition that converges to the classical simply supported plate model as the gradient parameter, g, goes to zero. It would be interesting to include more types of boundary conditions, such as singly and doubly clamped, double simply supported, and free boundaries. The boundary of the plate is limited to straight boundaries. Extending the current work to curved boundaries would significantly increase our understanding of the model and the algorithms. For the pie-shaped geometry, even though the reference solution and the solution from the direct method agree well, they are not the same. The difference measured in the H^3 norm becomes even more evident. The discrepancy might be caused by the singular parametrization of the geometry and by the singularity of the basis function at the singular point. Thus, it is necessary to develop basis functions that are H^3-conforming everywhere for such concave geometry.

ACKNOWLEDGEMENTS

We greatly appreciate the helpful comments from the reviewers, which lead to significant improvement of the manuscript.

APPENDIX A. CONVERGENCE RESULTS USING DIRECT METHOD

We present in this section convergence results obtained by solving the manufactured solution discussed in Section 4.1 using the direct method (Section 3.2). The gradient parameter is chosen to be $g = 0.01$. Convergence results using a B-spline basis of order $p = 3$, 4 and 5 are shown in Tables A.1, A.2 and A.3, respectively. Convergence rates are in agreement with [21].

Table A.1. Convergence results of w using the direct method (Section 3.2) with $p = 3$ and $g = 0.01$. Convergence rates are shown in the bracket.

N	$L^2(\Omega)$	$H^1(\Omega)$	$H^2(\Omega)$	$H^3(\Omega)$
2	$4.28 \times 10^{-3}(-)$	$4.53 \times 10^{-2}(-)$	$6.53 \times 10^{-1}(-)$	$1.02 \times 10^{1}(-)$
4	$3.59 \times 10^{-4}(3.58)$	$7.13 \times 10^{-3}(2.67)$	$1.71 \times 10^{-1}(1.93)$	$5.08 \times 10^{0}(1.00)$
8	$1.99 \times 10^{-5}(4.17)$	$8.06 \times 10^{-4}(3.14)$	$4.09 \times 10^{-2}(2.07)$	$2.50 \times 10^{0}(1.02)$
16	$1.55 \times 10^{-6}(3.68)$	$9.79 \times 10^{-5}(3.04)$	$1.01 \times 10^{-2}(2.02)$	$1.24 \times 10^{-1}(1.01)$

Table A.2. Convergence results of w using the direct method (Section 3.2) with $p = 4$ and $g = 0.01$. Convergence rates are shown in the bracket.

N	$L^2(\Omega)$	$H^1(\Omega)$	$H^2(\Omega)$	$H^3(\Omega)$
2	$1.34 \times 10^{-3}(-)$	$1.37 \times 10^{-2}(-)$	$1.81 \times 10^{-1}(-)$	$3.35 \times 10^{0}(-)$
4	$3.92 \times 10^{-5}(5.09)$	$7.85 \times 10^{-4}(4.12)$	$1.84 \times 10^{-2}(3.30)$	$5.92 \times 10^{-1}(2.50)$
8	$1.06 \times 10^{-6}(5.21)$	$4.62 \times 10^{-5}(4.09)$	$2.29 \times 10^{-3}(3.01)$	$1.33 \times 10^{-1}(2.15)$
16	$4.86 \times 10^{-8}(4.45)$	$2.94 \times 10^{-6}(3.97)$	$2.93 \times 10^{-4}(2.96)$	$3.20 \times 10^{-2}(2.06)$

Table A.3. Convergence results of w using the direct method (Section 3.2) with $p = 5$ and $g = 0.01$. Convergence rates are shown in the bracket.

N	$L^2(\Omega)$	$H^1(\Omega)$	$H^2(\Omega)$	$H^3(\Omega)$
2	$6.47 \times 10^{-5}(-)$	$1.02 \times 10^{-3}(-)$	$1.85 \times 10^{-2}(-)$	$4.63 \times 10^{-1}(-)$
4	$6.08 \times 10^{-6}(3.41)$	$1.33 \times 10^{-4}(2.94)$	$3.05 \times 10^{-3}(2.60)$	$7.33 \times 10^{-2}(2.66)$
8	$6.91 \times 10^{-8}(6.46)$	$3.31 \times 10^{-6}(5.33)$	$1.61 \times 10^{-4}(4.24)$	$8.00 \times 10^{-3}(3.20)$
16	$5.91 \times 10^{-9}(3.55)$	$9.99 \times 10^{-8}(5.05)$	$9.60 \times 10^{-6}(4.07)$	$9.65 \times 10^{-4}(3.05)$

APPENDIX B. CONVERGENCE RESULTS USING THE SPLIT METHOD FOR DIFFERENT g

We provide in this section convergence results of the additional variables, u_1 (Fig. B.1) and u_2 (Fig. B.2), using the split method for different gradient parameters, g. We use linear basis functions. Optimal convergence rates, second-order in the L^2 norm and linear in the H^1 norm, are obtained.

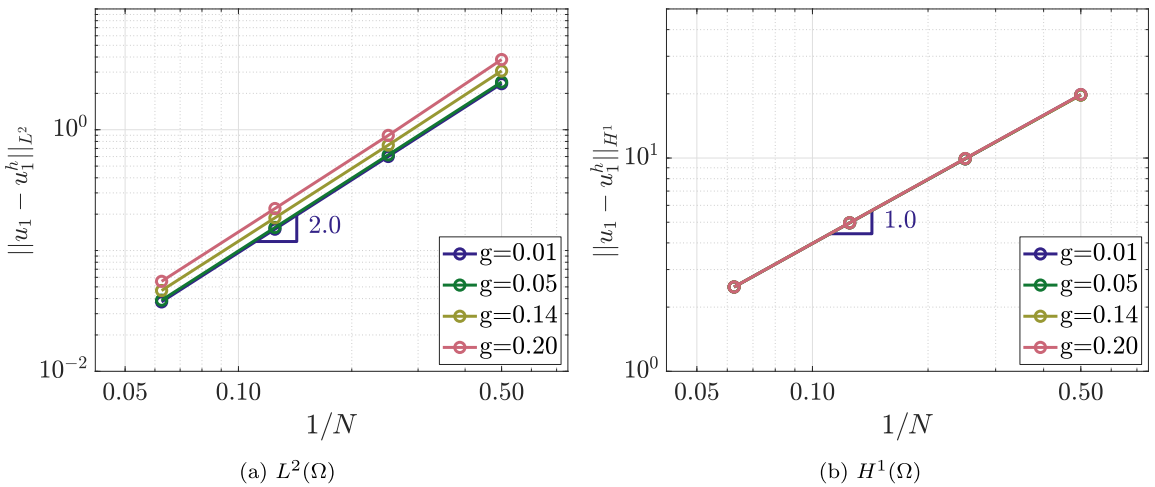

(a) $L^2(\Omega)$ (b) $H^1(\Omega)$

Figure B.1 Convergence results of u_1 in L^2 and H^1 norms using the split method (Section 3.3) with $p = 1$ and $g = 0.01, 0.05, 0.14, 0.2$.

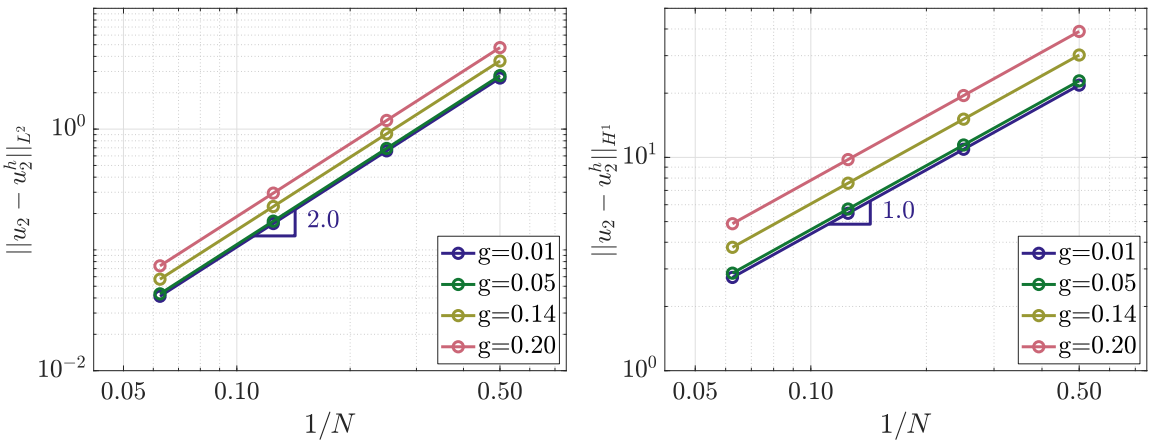

(a) $L^2(\Omega)$ (b) $H^1(\Omega)$

Figure B.2 Convergence results of $u_2 = -\Delta w + g^2\Delta^2 w$ in L^2 and H^1 norms using the split method (Section 3.3) with $p = 1$ and $g = 0.01$, 0.05, 0.14, 0.2.

REFERENCES

1. Malvern LE. *Introduction to the Mechanics of a Continuous Medium*. Englewood Cliffs, NJ: Prentice-Hall,1969.
2. Hughes TJ. *The Finite Element Method: Linear Static and Dynamic Finite Element Analysis*. Courier Corporation, 2012.
3. Holzapfel G. *Nonlinear Solid Mechanics. A Continuum Approach for Engineering*. 2nd print edn. New York: Wiley, 2001.
4. Connor JJ, Faraji S. *Fundamentals of Structural Engineering*. Berlin: Springer, 2013.
5. Leng Y, Ardekani AM, Gomez H. A poro-viscoelastic model for the subcutaneous injection of monoclonal antibodies. *Journal of the Mechanics and Physics of Solids* 2021;**155**:104537.
6. Leng Y, de Lucio M, Gomez H. Using poro-elasticity to model the large deformation of tissue during subcutaneous injection. *Computer Methods in Applied Mechanics and Engineering* 2021;**384**: 113919.
7. Dell'Isola F, Seppecher P, Alibert JJ, Lekszycki T, Grygoruk R, Pawlikowski M, Steigmann D, Giorgio I, Andreaus U, Turco E et al., Pantographic metamaterials: an example of mathematically-driven design and of its technological challenges. *Continuum Mechanics and Thermodynamics* 2019;**31**(4):851–884.
8. Makvandi R, Duczek S, Juhre D. A phase-field fracture model based on strain gradient elasticity. *Engineering Fracture Mechanics* 2019;**220**:106648.
9. Eringen AC, Suhubi E. Nonlinear theory of simple micro-elastic solids'i. *International Journal of Engineering Science* 1964;**2**(2):189–203.
10. Mindlin RD. Microstructure in linear elasticity. Technical report. Columbia University New York Department of Civil Engineering and Engineering Mechanics, 1963.
11. Askes H, Aifantis EC. Gradient elasticity in statics and dynamics: an overview of formulations, length scale identification procedures, finite element implementations and new results. *International Journal of Solids and Structures* 2011;**48**(13):1962–1990.
12. Aifantis EC. Strain gradient interpretation of size effects. *Fracture scaling*. Berlin: Springer, 1999, 299–314.
13. Carpinteri A. Higher order gradients and size effects. in *Size-Scale Effects in the Failure Mechanisms of Materials and Structures*. London: CRC Press, 2002, 245–256.
14. Zhu HT, Zbib H, Aifantis E. Strain gradients and continuum modeling of size effect in metal matrix composites. *Acta Mechanica* 1997;**121**(1):165–176.
15. Altan B, Aifantis E. On some aspects in the special theory of gradient elasticity. *Journal of the Mechanical Behavior of Materials* 1997;**8**(3):231–282.
16. Hughes TJ, Cottrell JA, Bazilevs Y. Isogeometric analysis: CAD, finite elements, NURBS, exact geometry and mesh refinement. *Computer Methods in Applied Mechanics and Engineering* 2005;**194**(39–41):4135–4195.
17. Gómez H, Calo VM, Bazilevs Y, Hughes TJ. Isogeometric analysis of the Cahn–Hilliard phase-field model. *Computer Methods in Applied Mechanics and Engineering* 2008;**197**(49–50):4333–4352.
18. Gomez H, Hughes TJ, Nogueira X, Calo VM. Isogeometric analysis of the isothermal Navier–Stokes–Korteweg equations. *Computer Methods in Applied Mechanics and Engineering* 2010;**199**(25-28):1828–1840.
19. Zareh M, Qian X, C1 triangular isogeometric analysis of the von karman equations. arXiv:2108.00971, 2021.
20. Hu T, Leng Y, Gomez H. A novel method to impose boundary conditions for higher-order partial differential equations. *Computer Methods in Applied Mechanics and Engineering* 2022;**391**:114526.
21. Niiranen J, Kiendl J, Niemi AH, Reali A. Isogeometric analysis for sixth-order boundary value problems of gradient-elastic Kirchhoff plates. *Computer Methods in Applied Mechanics and Engineering* 2017;**316**:328–348.
22. Thai S, Thai HT, Vo TP, Patel VI. Size-dependant behaviour of functionally graded microplates based on the modified strain gradient elasticity theory and isogeometric analysis. *Computers & Structures* 2017;**190**:219–241.
23. Babu B, Patel B. A new computationally efficient finite element formulation for nanoplates using second-order strain gradient Kirchhoff's plate theory. *Composites Part B: Engineering* 2019;**168**:302–311.
24. Liebold C, Dawwas BM. Numerical solution of the tri-harmonic Kirchhoff plate equation resulting from a strain gradient theory. *New Achievements in Continuum Mechanics and Thermodynamics* Cham: Springer, 2019, 271–290.
25. Zhang B, Li H, Kong L, Zhang X, Shen H. Strain gradient differential quadrature Kirchhoff plate finite element with the c2 partial compatibility. *European Journal of Mechanics-A/Solids* 2020;**80**:103879.
26. Ammar K, Appolaire B, Cailletaud G, Feyel F, Forest S. Finite element formulation of a phase field model based on the concept of generalized stresses. *Computational Materials Science* 2009;**45**(3):800–805.
27. Baňas L, Nürnberg R. A multigrid method for the Cahn–Hilliard equation with obstacle potential. *Applied Mathematics and Computation* 2009;**213**(2):290–303.
28. Barrett J, Blowey J. Finite element approximation of the Cahn–Hilliard equation with concentration dependent mobility. *Mathematics of Computation* 1999;**68**(226):487–517.

29. Elliott CM, French DA, Milner F. A second order splitting method for the Cahn–Hilliard equation. *Numerische Mathematik* 1989;**54**(5):575–590.
30. Elliott CM, Larsson S. Error estimates with smooth and nonsmooth data for a finite element method for the Cahn–Hilliard equation. *Mathematics of Computation* 1992;**58**(198):603–630.
31. Kim J, Kang K, Lowengrub J. Conservative multigrid methods for Cahn-Hhilliard fluids. *Journal of Computational Physics* 2004;**193**(2):511–543.
32. Xia Y, Xu Y, Shu CW. Local discontinuous Galerkin methods for the Cahn-Hhilliard type equations. *Journal of Computational Physics* 2007;**227**(1):472–491.
33. Gerasimov T, Stylianou A, Sweers G. Corners give problems when decoupling fourth order equations into second order systems. *SIAM Journal on Numerical Analysis* 2012;**50**(3): 1604–1623.
34. Nazarov SA, Sweers G. A hinged plate equation and iterated Dirichlet Laplace operator on domains with concave corners. *Journal of Differential Equations* 2007;**233**(1):151–180.
35. Sweers G. A survey on boundary conditions for the biharmonic. *Complex Variables and Elliptic Equations* 2009;**54**(2): 79–93.
36. Niiranen J, Niemi AH. Variational formulations and general boundary conditions for sixth-order boundary value problems of gradient-elastic Kirchhoff plates. *European Journal of Mechanics—A/Solids* 2017;**61**:164–179.
37. Mindlin RD, Second gradient of strain and surface-tension in linear elasticity. *International Journal of Solids and Structures* 1965;**1**(4):417–438.
38. Shkoller S. Mat201c lecture notes: Introduction to sobolev space. 2011.
39. Evans LC. *Partial Differential Equations, Graduate Studies in Mathematics* Vol. 19. Providence, RI: AMS, 2002.
40. Ladyzhenskaya O, Ural'tseva N. *Linear and Quasilinear Elliptic Equations* Vol. 19. New York: Academic Press, 1968.
41. Brenner SC, Scott LR. *The Mathematical Theory of Finite Element Methods* Vol. 3. New York: Springer, 2008.
42. Nazarov SA, Plamenevskiĭ BA. *Elliptic Problems in Domains with Piecewise Smooth Boundaries, De Gruyter Expositions in Mathematics*. Berlin: W. de Gruyter, 1994.
43. Kozlov VA, Maz'ya VG, Rossmann J. *Elliptic Boundary Value Problems in Domains with Point Singularities* Vol. 52. Providence, RI: American Mathematical Society, 1997.
44. Kunoth A, Lyche T, Sangalli G, Serra-Capizzano S. *Splines and PDEs: From Approximation Theory to Numerical Linear Algebra: Cetraro, Italy 2017, volume 2219 of Lecture Notes in Mathematics*. Cham: Springer, 2018.
45. Cottrell JA, Hughes TJ, Bazilevs Y, *Isogeometric Analysis: Toward Integration of CAD and FEA*. New York: Wiley, 2009.
46. Kästner M, Metsch P, de Borst R. Isogeometric analysis of the Cahn–Hilliard equation—a convergence study. *Journal of Computational Physics* 2016;**305**:360–371.